Nanochem Res 8(2): 95-105 Spring 2023

RESEARCH PAPER

Efficiency of Melamine Grafted Chitosan-based Magnetic Nanocomposite for Cationic Dye Adsorption: Kinetics, Isotherms, Thermodynamics

Hossein Dehghani, Sanaz Sajedi- Amin*, Abdolhossein Naseri*

Department of Analytical Chemistry, Faculty of Chemistry, University of Tabriz, Tabriz, Iran

ARTICLE INFO

Article History:
Received 06 Nov 2022
Accepted 26 Dec 2022
Published 06 Mar 2023

Keywords:
Chitosan
Fe_3O_4 nanoparticles
Melamine
Dye pollutants
Magnetic sorbent
Dye removal

ABSTRACT

The adsorption activity of functionalized magnetic nanoparticles with chitosan-melamine as a sorbent were studied for the removal of dye contaminants from aqueous solution. The morphology, structure, and size of the MA-CS@Fe_3O_4 nanocomposite were investigated. The synthesized pH-sensitive adsorbent successfully adsorbs cationic dyes such as basic red and methyl blue. Adsorption experiments were carried out as batch studies at different contact times, pH, initial dye concentrations, and adsorbent dosages. The dye adsorption equilibrium was rapid as it was achieved under 30 min of contact time with 5 mg adsorbent. The equilibrium data were analyzed by nonlinear Langmuir and Freundlich model for BR and MB adsorption. The best fitting results were achieved for Langmuir model which confirm that the adsorption of dyes is monolayer and the surface of MA-CS@Fe_3O_4 sorbent is homogeneous. The pseudo-second-order kinetics can describe the adsorption process for both MB and BR. The thermodynamic analysis indicated that the adsorption was a spontaneous and endothermic process.

How to cite this article
Dehghani H., Sajedi- Amin S., Naseri A., Efficiency of Melamine Grafted Chitosan-based Magnetic Nanocomposite for Cationic Dye Adsorption: Kinetics, Isotherms, Thermodynamics. Nanochem Res, 2023; 8(2): 95-105
DOI: 10.22036/ncr.2023.02.002

INTRODUCTION

Environmental protection has received a great deal of attention in the last few years. One of the environmental issues today is colored wastewater from several manufacturing industries such as leather, dye, plastic, textile, which has detrimental impacts on aquatic life and is carcinogenic for human health [1, 2]. Most of dyes are water soluble and quite difficult to degrade since the aromatic ring of azo dyes is hard to break [3]. In addition, a small amount of dye in water is undesirable and needs to be removed. Adsorption process is more appealing to be used when compared to other conventional methods, such as coagulation and flocculation [4, 5], oxidation or ozonation [6, 7], membrane separation [8], for removing dye from wastewater, because of its simplicity of operation, high removal efficiency, and reusability of adsorbents [9]. Various types of adsorbents including metal-organic frameworks [10], carbon-based hybrid materials[11], polymer based nanocomposites [12], and metal oxide-based hybrids were used for efficient dyes removal [13].

In recent years, environmentally friendly adsorbents have steadily made progress. Chitosan (CS)-based nanocomposites are more favorable due to their perfect physicochemical properties such as biocompatibility, nontoxicity, reactive enriched surface, and cost-effectiveness [14]. Several functional groups on chitosan provide chemical modification for improving its weak spots owning to low surface area, low porosity, and

* Corresponding Author Email: *a_naseri@tabrizu.ac.ir*
sv.sajedi@gmail.com

poor mechanical properties [15]. Using melamine (MA) as surface modifier has led to important breakthroughs, resulting in nanosorbents with special features and functionalities [16]. On the other hand, a combination of magnetic Fe_3O_4 nanoparticles with polymer-based nanosorbents will be conducive to an efficient and rapid separation process through the dye removal processes [17-19]. Therefore, the purpose of this work was to use functionalized magnetic nanoparticles with chitosan-melamine for studying the removal of dye contaminants from aqueous solutions.

MATERIALS AND METHODS

Chemicals and Materials

CS, MA, and epoxy chloropropane was purchased from Sigma-Aldrich. Fe_3O_4 (98% purity, 20-30 nm) was obtained from IR Nanomaterials Pioneers Inc. (NANOSANY Co.). All other reagents were analytical grade and used without further purification. Deionized water was used in the preparation of all solutions. The cationic dye used in the tests was the analytical reagent. Basic red (BR) and methyl blue (MB) was obtained from the Sigma-Aldrich.

Instrumentation

All spectral measurements were carried out using a double beam UV/Vis spectrophotometer model UV-1601 PC (SHIMADZU, Kyoto, Japan). The pH studies were performed with a Metrohm 713 pH-meter combined glass electrode (Herisau, Switzerland). Mechanical stirring was conducted throughout the work using a Heidolph RZR 2102 Control Overhead Stirrer (Schwabach, Germany).

The scanning electron microscopy (SEM; FEG-SEM MIRA3 TESCAN, Brno, Czech Republic) was implemented for determining the size and morphology of synthesized magnetic sorbent. The functional groups of the samples were characterized using Fourier transform infrared (FTIR) spectroscopy (Bruker Tensor 27 spectrometer, Ettlingen, Germany), and the magnetic properties of the synthesized magnetic nano-sorbent was determined using a vibrating-sample magnetometer (VSM; AGFM, Tehran, Iran). The size and zeta-potential of samples were measured with laser-scattering techniques (Zeta sizer Nano ZS90; Malvern Instruments, Malvern, UK). The thermogravimetric analysis (TGA) of NPs was carried out with a Mettler-Toledo model 822 instrument (Schwerzenbach, Switzerland).

Preparation of MA-CS@Fe_3O_4

The preparation of magnetic melamine grafted chitosan was inspired by *Wu et.al.* with a few minor modifications [19]. The first step of the synthesis is dissolving a certain amount (0.2 g) of CS in 20 mL acetic acid solution (2 %w/w) and stirring for 2 h. The prepared solution was added dropwise into NaOH (0.25 mol L^{-1}, 20 mL) under stirring. After the precipitation was completed, the solution was filtered and the white precipitant was washed with acetone. The obtained solid was transferred to acetone (20 mL) and stirred to get homogeneous suspension. Epoxy chloropropane (1 mL) as a cross linker was added to the above CS suspensions and stirred at 298 K for 24 h. Then, Fe_3O_4 nanoparticles were introduced to the mixture with continuous ultrasonic dispersion for 20 min. After that, MA (1.10 g) dissolved in DMSO (10 mL) was added and refluxed for 7 h at 338 K. Then, the products were again mixed with 10 mL MA in DMSO, NaOH (1.00 mol L^{-1}, 10 mL), and KI (0.01 g), respectively, and stirred for 5 h. In this step CS was cross-linked with MA in alkaline solution through the active amino and hydroxyl groups in polymer chains of CS and MA to generate the compact composite network. The product was filtered and washed several times with deionized water and acetone. The final product was dried in a vacuum oven at 333 K. The schematic of the synthesized MA-CS@Fe_3O_4 nanocomposite is shown in Fig. 1.

Adsorption studies of basic red and methyl blue

The proper amount of the synthesized adsorbent was added to 10 mL individual water solution of each dye (BR or MB). After pH adjustment by adding 1 mol L^{-1} solution of HCl or NaOH, the solution was stirred on a shaker for 5 min. The magnetic nanosorbent was separated rapidly using a strong neodymium-iron-boron (NdFeB) magnet. The residual concentration of dye solution was determined using a calibration curve prepared at the corresponding wavelength (465 nm for BR and 520nm for MB) employing a UV–visible spectrometer. The amount of adsorbed dye (q_e, mg/g) was calculated by the following equation:

$$q_e = \frac{(C_0 - C_e)V}{W} \quad (1)$$

Where C_o and C_e are the initial and final (equilibrium) concentrations (mg/L), respectively. V is the volume of dye solution (L), and W is the weight (g) of MA-CS@Fe_3O_4 adsorbent. The

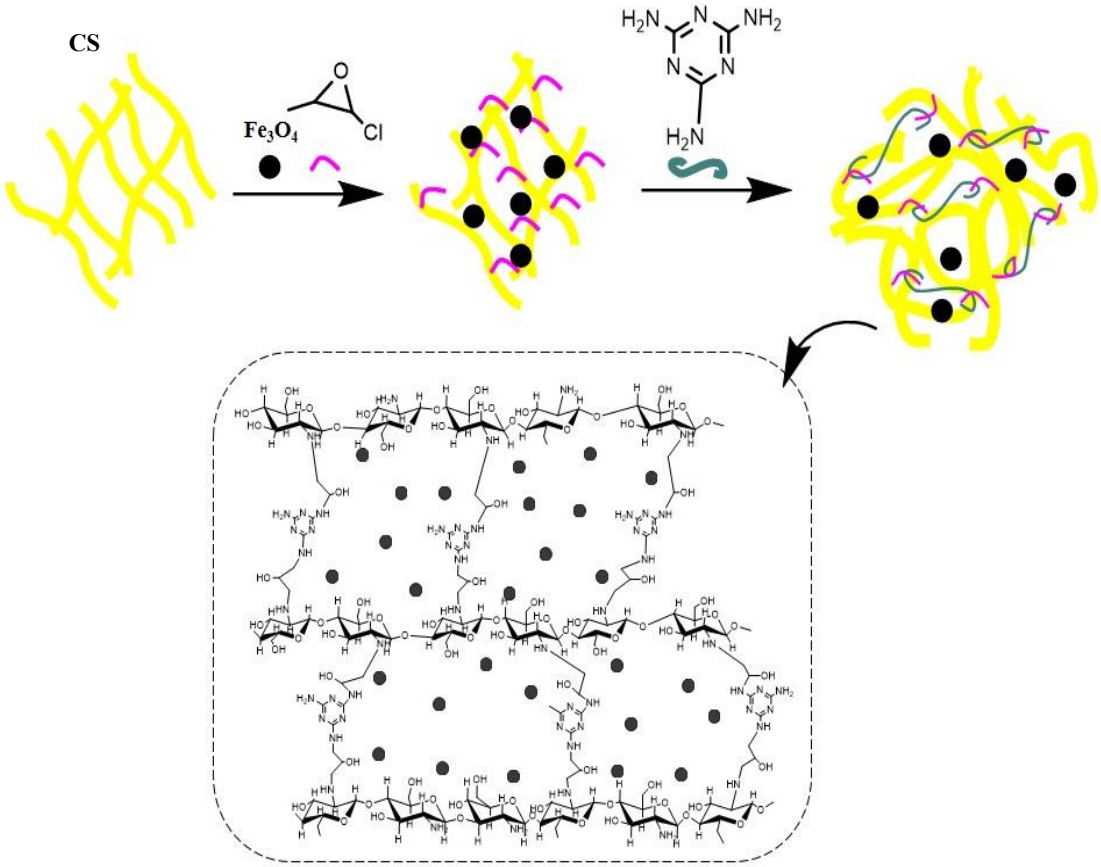

Fig. 1. Schematic of synthesize MA-CS@Fe_3O_4 nanocomposite

dye removal efficiencies, R%, were expressed in percentage as follows:

$$\%R = \frac{(C_0 - C_e)}{C_0} \times 100 \quad (2)$$

The effect of different experimental conditions (initial concentration of dye, pH, contact time and amount of adsorbent) on the efficient adsorption of studied cationic dyes (i.e. BR and MB) with MA-CS@Fe_3O_4 adsorbent from aqueous solutions was investigated. The effect of pH on dye removal was studied over a pH range of 3 to 9. The concentration of BR and MB dye solutions ranged from (3 to 12) and (5 to 15) mg/L, respectively, to investigate the adsorption isotherms. The sorption studies were also carried out at different temperatures (25-60 °C) to determine the effect of temperature.

RESULTS AND DISCUSSION

Characterization

Fig. 2 presents the IR spectrum of CS, MA, and MA-CS@Fe_3O_4 nanosorbent. Due to the chemical structure of the melamine molecule, we expect the presence of different functional groups such as C-N, C = N, NH2, and the triazine ring to be visible in its FT-IR spectrum. In general, the narrow N-H stretching vibration is observed at 3345, 3735, 3761, and 3851 cm^{-1}. However, the broad peak in the chitosan spectrum (a) in region 3464 cm^{-1} is related to the stretching vibrations of the hydroxyl group, which is mounted on the N-H peak in the spectrum of the synthesized nanocomposite. The bifurcation peak at 1552 cm^{-1} is related to the bending vibrations of the N-H bond in melamine, which appeared in the IR spectrum of melamine and synthesized MA-CS@Fe_3O_4 nanoadsorbent; however, the peak related to the bending vibrations of the O-H bond in chitosan appeared at 1660 cm^{-1}. Stretching vibrations in the range 1552-1340 cm^{-1} are attributed to the triazine ring, which are visible in the synthesized sample and melamine. The peak of the twisting vibrations of the N-H bond in the range of 1162-1026 cm^{-1} is visible for the synthesized material and melamine. The characteristic peak at

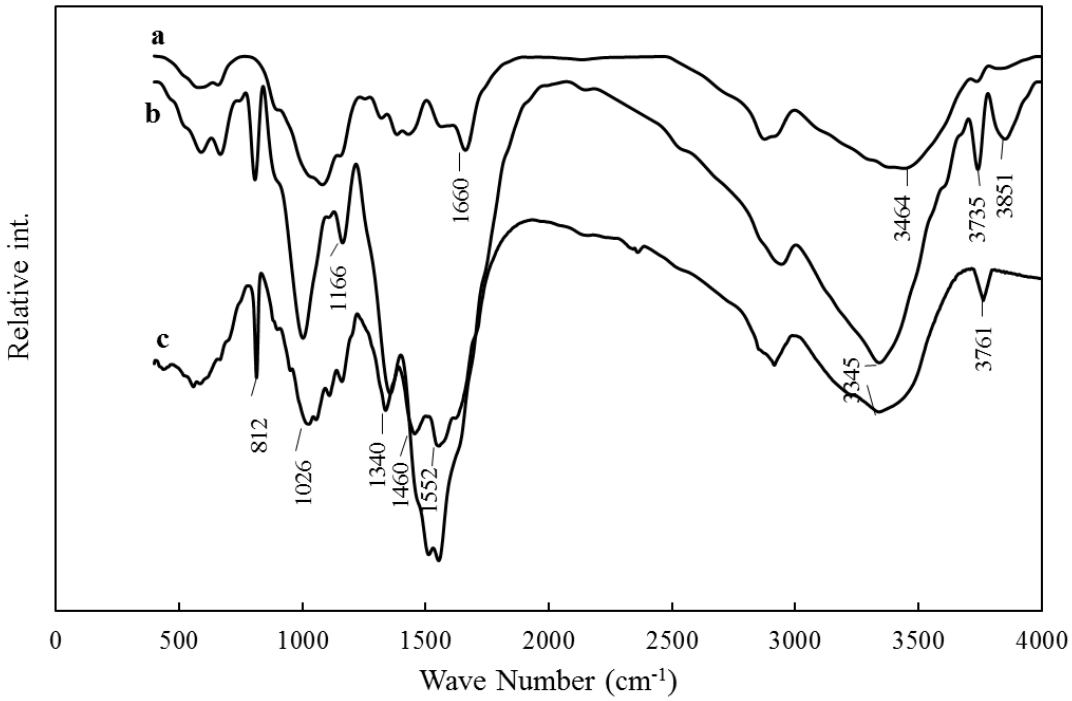

Fig. 2. IR spectra of CS (a), MA (b) and MA-CS/Fe_3O_4 (c).

812 cm^{-1}, which belongs to the distorting vibrations of the triazine ring, also appeared in the melamine and the synthesized sample and provided evidence for our synthesis.

The surface morphology of the MA-CS@Fe_3O_4 was revealed by SEM, as shown in Fig. 3a,b. The SEM images indicated a rough morphology with a little aggregative phenomenon in the Fe_3O_4–chitosan nanoparticles.

Size distributions were determined by DLS (Fig. 3c) in aqueous solution. The average size of the MA-CS@Fe_3O_4 nanoparticles (Fig. 3c) ranged 88.04±12.99 nm which is larger than the size of naked Fe_3O_4 nanoparticles (39.01±8 nm). This revealed that the coating process is done successfully. The energy dispersive X-ray (EDX) spectrum of the MA-CS@Fe_3O_4 along with naked Fe_3O_4 nanoparticles are showed in Fig. 4. Through EDX, no peaks other than those of carbon, nitrogen, oxygen, and iron confirm that the designed catalyst is successfully synthesized and the Fe_3O_4 nanoparticles is successfully loaded.

Furthermore, the zeta potential data was measured at different pH values at room temperature (Fig. 5a). As the results indicate, high levels of amino, imino, and hydroxyl groups can be found in MA-CS@Fe_3O_4. Due to electrostatic repulsion, the majority of these groups were easily protonated at low pH levels, which made it difficult to adsorb cationic dyes. These led to the reduction of adsorbent's adsorption capability. The de-protonation was enhanced by the rise in pH. In addition, at higher pH levels, iron oxides' surfaces would transform to functional groups of FeO^- and their surface zeta potential would shift to the negative. Thus, the MA-CS@Fe_3O_4 is more suited for cationic dyes such as basic red and methyl blue adsorption at high pH levels [20, 21]. However, the pH at the zero-point charge is a highly important experimental characteristic that shows the net electrical neutrality for any particular adsorbent. In this work, as shown in Fig. 5a, the measurements indicate a zero charge at pH 3.3 and positive surface of adsorbent at pH values below the zero point.

TGA analysis of MA-CS@Fe_3O_4 is shown in Fig. 5b. As shown, the weight loss of MA-CS/Fe_3O_4 over the temperature range from 25 to 220 °C is about 10% due to the water loss of the sample. When the temperature was raised to 500 °C, the organic decomposition step occurred and the weight loss was 66.26%. The Fe_3O_4 in MA-CS/Fe_3O_4 could not be oxygenated under nitrogen atmosphere. In fact, no obvious change in mass content will be expected over a 500 °C.

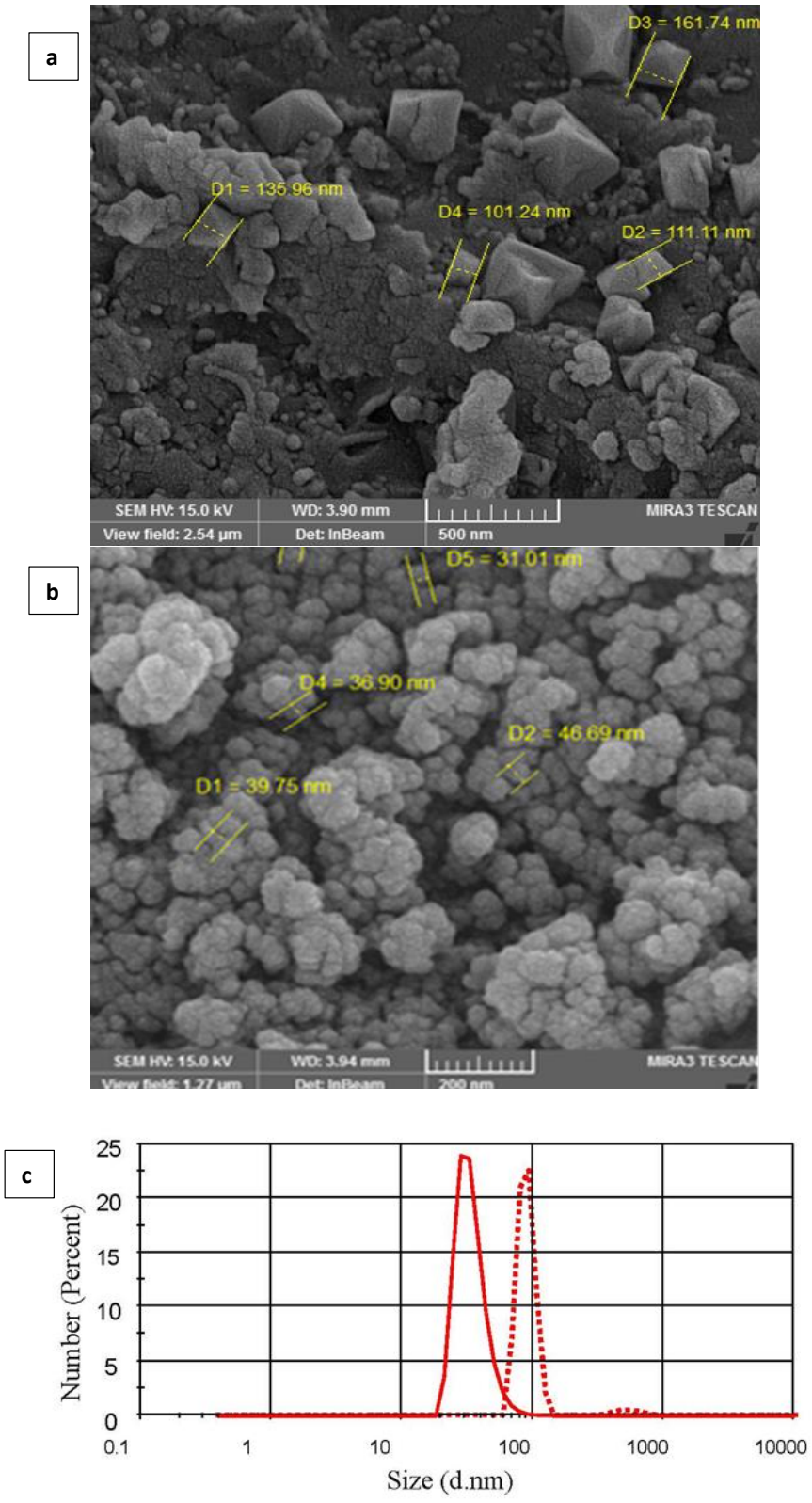

Fig. 3. SEM analysis of a) MA-CS@Fe_3O_4 and b) naked Fe_3O_4 and average size distribution using DLS for c) MA-CS@Fe_3O_4 nanosorbent (…) and naked Fe_3O_4 (—).

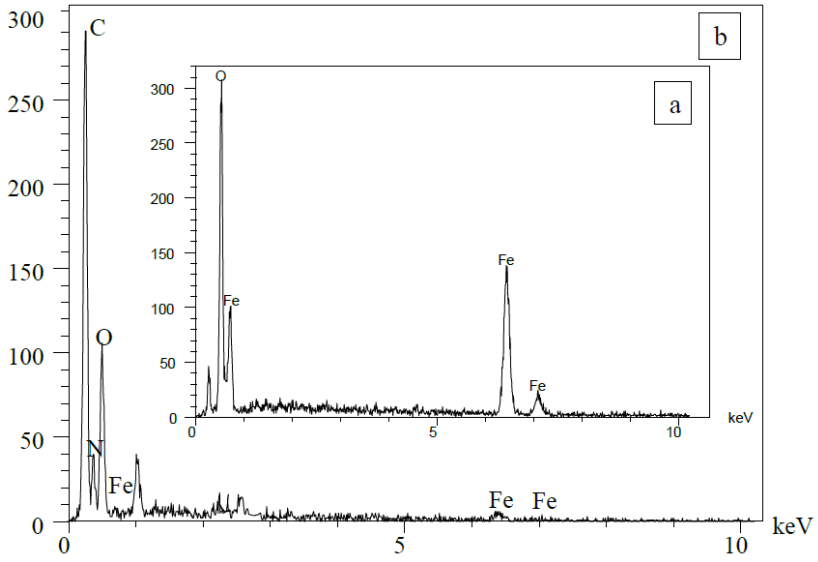

Fig. 4. Energy dispersive spectroscopy (EDX) pattern of (a) Fe_3O_4 particles, (b) MA-CS@Fe_3O_4.bent (…) and naked Fe_3O_4 (—).

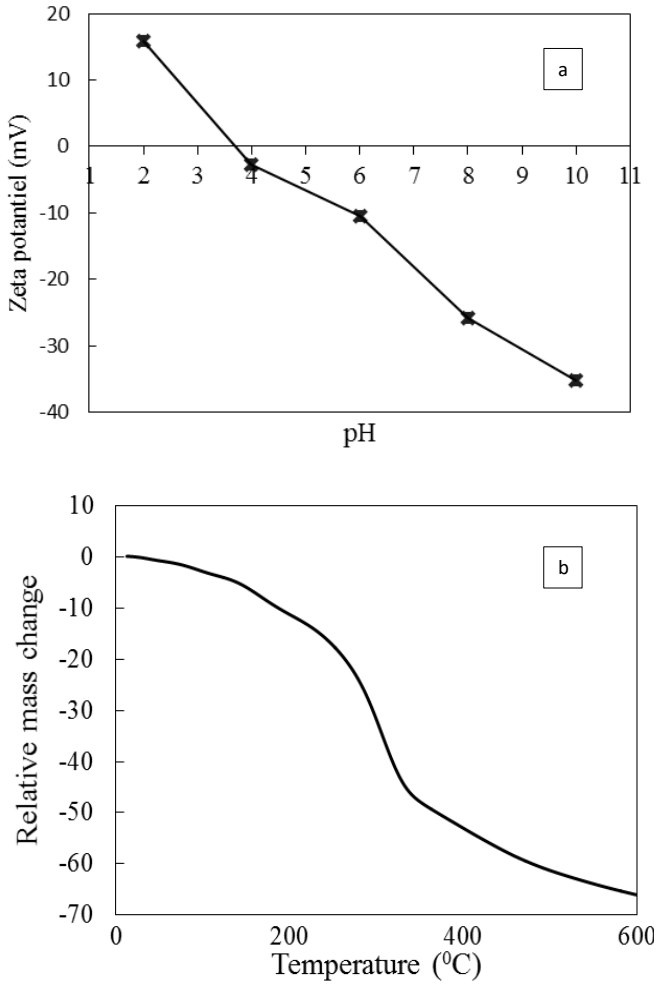

Figure 5. a) Zeta potential and b) TGA analysis of MA-CS@Fe_3O_4

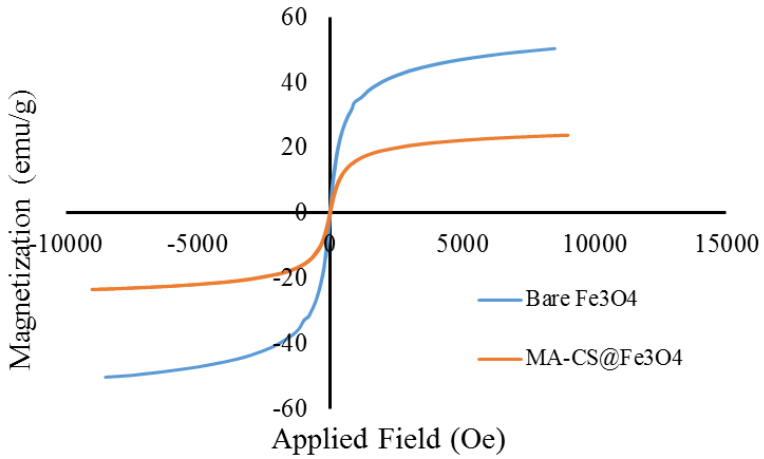

Fig. 6. The VSM results for bare Fe_3O_4 and MA-CS@Fe_3O_4

The magnetic properties of the synthesize nanosorbent were studied using VSM (vibrating sample magnetometry) analysis. As can be seen in Fig. 6, the saturation magnetization values (Ms) were 50 and 23 for bare Fe_3O_4 and MA-CS/Fe_3O_4, respectively. The reduction of magnetism in MA-CS/Fe_3O_4 is due to the binding of melamine and chitosan. However, the synthesized magnetic nanosorbent still possessed high magnetic properties under an external field and could be easily separated from analyte solution in the shortest possible time (<10 s) and then with slightly shake can be readily redispersed.

Study of experimental parameters on the adsorption process

To study the effect of initial concentration on removal efficiency of dye, the initial concentration was varied in the range of 1-20 mg/L for MB and 5-20 mg/L for BR. It was observed that the dye removal efficiency reached up to about 80% at lower concentrations (5 mg/L in BR and 1 mg/L in MB), then decreased to 50% at higher concentrations (20 mg/L in BR and 15 mg/L in MB). The higher dye removal efficiency in low initial concentration is due to the availability of unoccupied binding sites of MA-CS@Fe3O4 adsorbent. The optimal initial concentration was selected 5 ppm for MB and 15 ppm for BR in the following studies.

The pH, as one of the important controlling factors, was investigated in the range of 2–10. The results of BR and MB were shown in Fig. 7. It is evident that with increasing pH, highest dye removal efficiencies were obtained. At low pH, the amino and hydroxyl groups are protonated on the nanosorbent's surfaces, while at high pH, these groups become deprotonated . The resulting negatively charged zeta potential (Fig.5a) on the nanoparticle surface can be attributed to the hydroxyl bonds of linker (epoxy chloropropane). Since the dye removal efficiencies remained almost constant in the pH range of 8-12, pH=8 was chosen as the optimum pH in the subsequent studies.

As seen in Fig. 8, the adsorbent dosage has a significant effect on the adsorption of dyes. It can be seen that the dye removal efficiency has the same trend for both studied dyes. The R% was quite rapid up to 5 mg, then no obvious change in the adsorption of dyes was observed. This suggests that at low dosages, binding sites or accessible surface functional groups are not adequate for the solution concentration of either MB or BR. Thus, 5 mg of MA-CS@Fe3O4 was taken as the optimum dosage in batch adsorption experiments.

The effect of contact time on the MB and BR removal efficiencies of magnetic nano-sorbent was also evaluated. This study was performed under optimum conditions (MB; 5 mg of sorbent, pH 8.0, initial dye concentration 5mg.L^{-1} and BR; 5 mg of sorbent, pH 8.0, initial dye concentration 15 mg.L^{-1}) for both cationic dyes. Fig. 9 represents a gradual increase in the dye removal efficiencies with the increase in the reaction contact time for both MB and BR. This behavior may be due to the rapid and efficient binding process between dyes and the active surface sites of the sorbent. In other words, the MB removal reaches to its maximum value after 5 min and then remains constant while this time for BR is 30 min. This maximum value is the equilibrium time, that is, the time for an

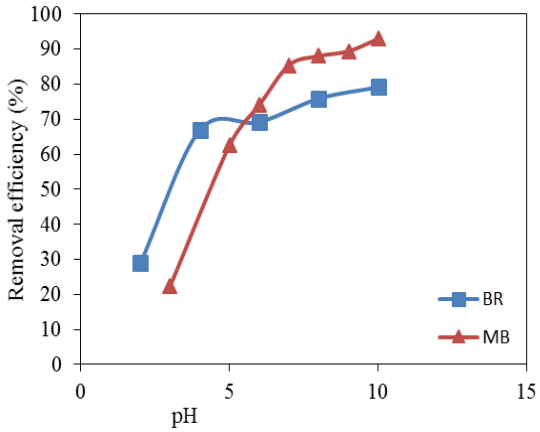

Fig. 7. Effect of pH on cationic dye adsorption. Experimental condition (the initial concentration is 5 mg/L and 15 mg/L for MB and BR respectively, the temperature was 25 °C, the amount of sorbent is 4 mg , volume of solution was 3 mL and the adsorption contact time was 30 min)

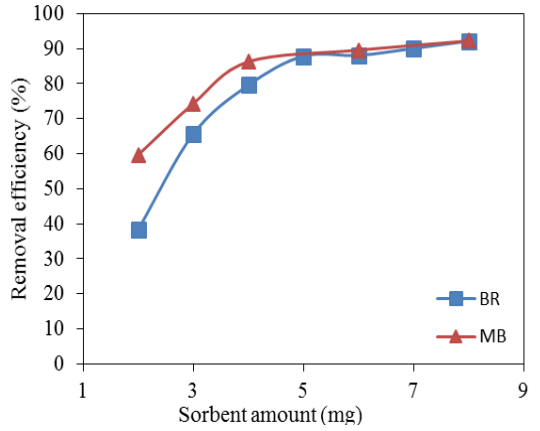

Fig. 8. Effect of sorbent amount on cationic dye adsorption at pH value of 8 and other experimental conditions are same as Fig. 6.

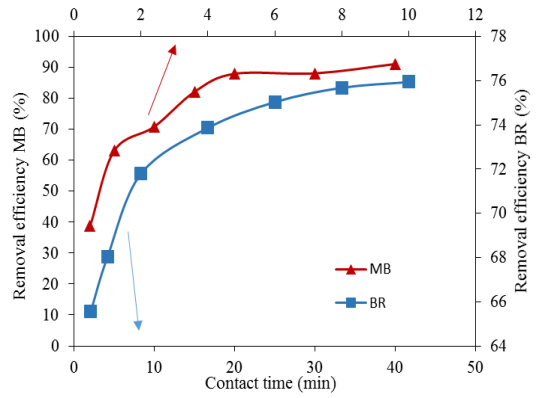

Fig. 9. Effect of contact time on cationic dye adsorption at pH value 8 and 5 mg of sorbent. Other experimental conditions are same as Fig. 6.

equilibrium to be established between sorbent's active sites and dyes in solution.

Adsorption isotherms

The performance of an adsorbent can be evaluated by adsorption isotherm data. Since it is not possible to find out the maximum amount of adsorption through experimental studies, it is useful to employ mathematical isothermal models proposed by researchers. Further, adsorption isotherm data is vital for the optimization of the adsorption pathway and effective design of the adsorption process. Two commonly used isotherm models, such as Langmuir and Freundlich were studied here. These isotherms are nonlinear models which describe the adsorption at defined pH and temperature. However, using the linear analysis of isotherm data as an alternative procedure is more appealing; however, the unreliable prediction of adsorption parameters with high uncertainties led to the exclusive use of nonlinear isotherm models. Langmuir isotherm model assumes that the surface of a solid is a perfectly uniform and homogeneous surface and any active cites does not absorb more than one molecule. Under such circumstances, monolayer adsorption occurs on the surface of the sorbent. The non-linear Langmuir isotherm model is expressed by the following equation:

$$q_e = q_m K_L \frac{C_e}{1 + K_L C_e} \quad (3)$$

Where C_e represents the concentration of dye at equilibrium (ppm); q_e denotes the amount of dye adsorbed at equilibrium (mg/g); q_m (mg/g) and K_L (L/mg) are model parameters which are related to adsorption capacity and energy or net enthalpy of adsorption, respectively.

The Freundlich isotherm is another model which can be applied to multilayer and heterogeneity adsorption. The non-linear expression of Freundlich isotherm model can be shown by the following equation (4):

$$q_e = K_F C_e^{\left(\frac{1}{n}\right)} \quad (4)$$

Where n and K_F are the model constants, indicating the surface heterogeneity and adsorption capacity, respectively.

The obtained equilibrium data were analyzed by nonlinear isotherms for BR and MB adsorption on synthesized sorbent. The values of corresponding isotherm parameters and related standard errors (S. E.) along with their correlation coefficients (R^2) are shown in Table 1. The highest R^2 values for MB

Table 1. Adsorption isotherm parameters for the adsorption of cationic dye onto MA-CS/Fe_3O_4 .

NO.	Isotherm model	Parameters	MB			BR		
			Values	S. E.	R^2	Values	S. E.	R^2
1	Langmuir	q_m (mg/g)	8.66	0.56	0.9866	3.67	0.07	0.9953
		K_L (L/mg)	0.53	0.10		1.75	0.16	
2	Freundlich	K_F (mg/g)	3.26	0.40	0.9409	2.19	0.16	0.9436
		n (g/L)	2.47	0.51		3.87	0.76	

(0.9866) and BR (0.9953) were obtained in fitting the data to the Langmuir isotherm model. It confirms that the adsorption of dyes is monolayer and the surface of MA-CS@Fe_3O_4 sorbent is homogeneous. The maximum monolayer adsorption capacity (q_m) was found to be 8.66 mg/g and 3.67 mg/g for the adsorption of MB and BR onto sorbent, respectively. The Langmuir favorable adsorption can be expressed with dimensionless parameter of R_L by the following equation:

$$R_L = \frac{1}{1 + K_L C_0} \quad (5)$$

Where C_0 is the initial dye color concentration (mg/L) and K_L the Langmuir's adsorption constant (L/mg). Where $R_L > 1$ unfavorable, $R_L = 1$ linear, $0 < R_L < 1$ favorable, $R_L = 0$ irreversible. The calculated R_Ls are in the range of 0.11-0.27 and 0.04-0.16 for MB and BR, respectively, which indicates the favorable adsorption process.

Adsorption kinetics

Kinetic studies were used to determine the adsorption rate and capacity of MB and BR on the synthesized adsorbent. Here, two well-known kinetic models of pseudo-first-order equation and pseudo-second-order equation according to equations 6 and 7 were used and the results are shown in Fig. 10.

$$\ln(q_e - q_t) = \ln q_e - t\,k_1 \quad (6)$$

$$\frac{t}{q_t} = \frac{1}{k_2 q_e^2} + \frac{t}{q_e} \quad (7)$$

Where q_e and q_t are the amounts of dye adsorbed (mg/g) at equilibrium and time (t), respectively; and k_1 (min^{-1}) and k_2 (g mg^{-1} min^{-1}) are the rate constant of the related equations. The best model will be selected with high coefficient of determination (R^2) for the adsorption. The fitting kinetic curves of these kinetic equations demonstrate that the pseudo-second-order kinetics can describe the adsorption process for both MB and BR. Through second-order kinetic model, chemical sorption involving valence forces describe the interaction between cationic dyes and MA-CS@Fe3O4.

Thermodynamic parameters

The thermodynamic parameters including the changes in standard enthalpy (ΔH^0, J mol^{-1}), free energy changes (ΔG^0, J mol^{-1}), and entropy change (ΔS^0, J $mol^{-1}K^{-1}$) were calculated for the adsorption of MB and BR on MA-CS@Fe_3O_4 and are listed in Table. 2.

$$k_d = \frac{q_e}{C_e} \quad (8)$$

$$\ln k_d = \frac{-\Delta G^\circ}{RT} \quad (9)$$

$$\Delta G^0 = -RT ln k_d = \Delta H^\circ - T\Delta S^\circ \quad (10)$$

Where R (8.314 J mol^{-1} K^{-1}) denotes the gas constant; T (K) is the absolute solution temperature, and k_d represents the thermodynamic equilibrium constant. The values of ΔH^0 and ΔS^0 were calculated from the slope and intercept of Van't Hoff equation (Eq. 9), where obtained with plotting lnk_d . 1/T. According to the results presented in Table.2, the negative free energy changes (ΔG^0) indicates that the adsorption of MB and BR onto adsorbent was thermodynamically spontaneous in the studied temperatures. The positive value of ΔH^0 further reveals that the adsorption is an endothermic process, indicating that the adsorption process for both MB and BR enhances with an increase in temperature. The positive ΔS showed the increase of randomness in the adsorption process.

Reusability of MA-CS@Fe_3O_4

The reusability of adsorbents is an essential parameter due to its economic benefits. The effect of recycling times of MA-CS@Fe_3O_4 on adsorption process was evaluated. The adsorption experiments were performed under optimum conditions for each dye. After each adsorption experiment, the adsorbent was recovered by 1 mol L^{-1} HCl solution

Table 2. Thermodynamic parameters for the adsorption of MB and BR on MA-CS/Fe_3O_4 .

	ΔG^0(J mol^{-1})					ΔH^0 (J mol^{-1})	ΔS^0(J $mol^{-1}K^{-1}$)
	293 K	303 K	313 K	323 K	333 K		
MB	-3816.60	-4564.68	-5450.04	-5795.61	-6292.57	14376.72	62.49
BR	-1467.23	-1924.52	-2776.15	-3000.55	-3339.63	13299.98	50.06

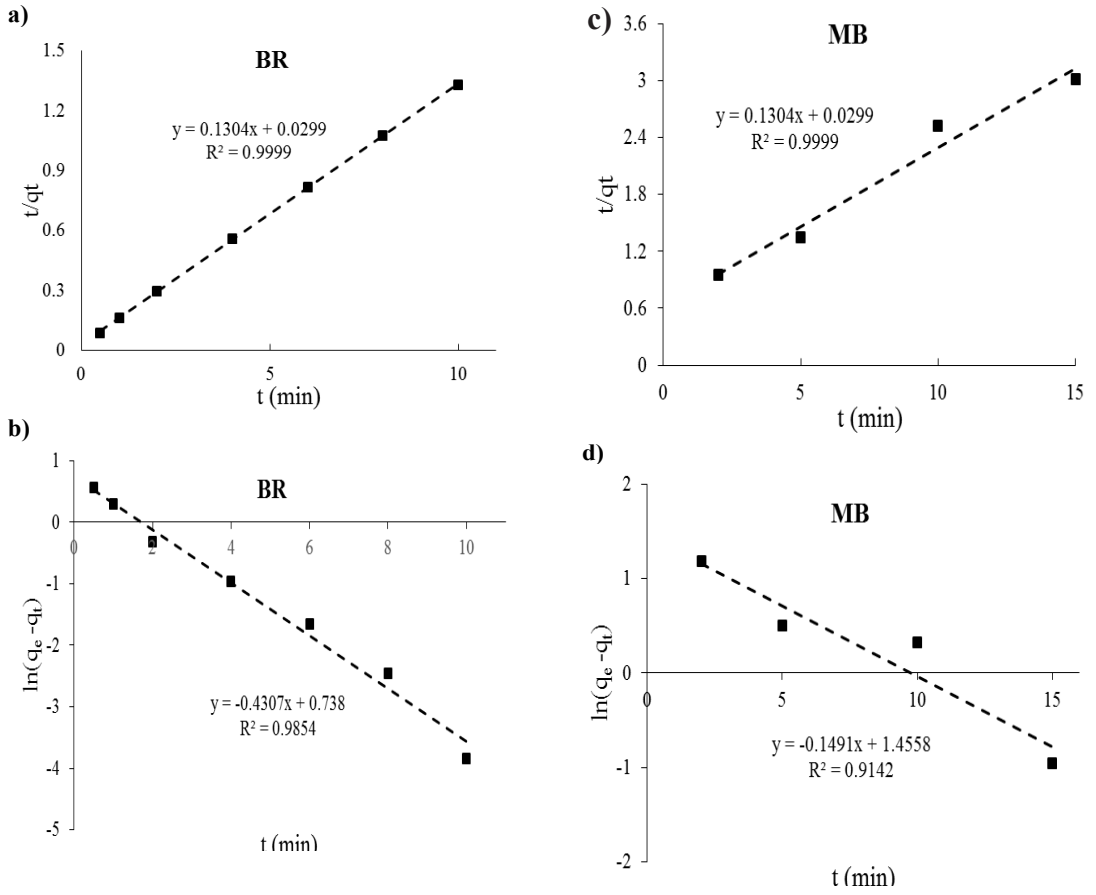

Fig. 10. (a), (c) pseudo- second-order and (b), (d) pseudo-first-order kinetic models for adsorption of BR and MB on MA-CS@Fe_3O_4.

and washed several times with 0.1 mol/L NaOH solution and distilled water, then dried and reused. The result implies that the removal efficiency of dyes dropped by 50 % by the 7th cycle, which may be due to the irreversible adsorption on the active sites of the adsorbent.

CONFLICT OF INTEREST

The authors declare no conflicts of interest.

CONCLUSIONS

Magnetic nanoadsorbents offers a new approach to overcome the problem of large amounts of sludge remaining in the use of conventional methods. Chitosan-based magnetic nanoadsorbents as an efficient ecofriendly material were employed in this study, allowing for preparing an adsorbent with special benefits such as easy collectability, regenerability, eco-friendliness, being economical, and having a large surface area. We successfully synthesized the functionalized magnetic nanoparticles with melamine grafted chitosan for efficient removal of dye contaminants from aqueous solutions. Bach experiments were conducted at different contact time, pH, initial dye concentration, and adsorbent dosage. The dye adsorption equilibrium was rapid as it was achieved under 5 min for MB and 30 min for

BR. The adsorption followed the pseudo-second order kinetic and Langmuir isotherm models. The adsorption process for both MB and BR rises with an increase in temperature. The regeneration and reusability of MA-CS@Fe_3O_4 has satisfactory removal efficiency of dyes after the 7th cycle.

REFERENCES

1. Mahmoodi NM, Salehi R, Arami M, Bahrami H. Dye removal from colored textile wastewater using chitosan in binary systems. Desalination. 2011;267(1):64-72. https://doi.org/10.1016/j.desal.2010.09.007
2. Saravanan A, Senthil Kumar P, Jeevanantham S, Karishma S, Tajsabreen B, Yaashikaa PR, et al. Effective water/wastewater treatment methodologies for toxic pollutants removal: Processes and applications towards sustainable development. Chemosphere. 2021;280:130595. https://doi.org/10.1016/j.chemosphere.2021.130595
3. Lellis B, Fávaro-Polonio CZ, Pamphile JA, Polonio JC. Effects of textile dyes on health and the environment and bioremediation potential of living organisms. Biotechnology Research and Innovation. 2019;3(2):275-90. https://doi.org/10.1016/j.biori.2019.09.001
4. Zhao C, Zheng H, Sun Y, Zhang S, Liang J, Liu Y, et al. Evaluation of a novel dextran-based flocculant on treatment of dye wastewater: Effect of kaolin particles. Science of The Total Environment. 2018;640-641:243-54. https://doi.org/10.1016/j.scitotenv.2018.05.286
5. McYotto F, Wei Q, Macharia DK, Huang M, Shen C, Chow CWK. Effect of dye structure on color removal efficiency by coagulation. Chemical Engineering Journal. 2021;405:126674. https://doi.org/10.1016/j.cej.2020.126674
6. García-Morales MA, Roa-Morales G, Barrera-Díaz C, Martínez-Miranda V, Balderas-Hernández P, Pavón T. Integrated Advanced Oxidation Process (Ozonation) and Electrocoagulation Treatments for Dye Removal in Denim Effluents. International Journal of Electrochemical Science. 2013;8:8752-63.
7. Arslan I. Treatability of a simulated disperse dye-bath by ferrous iron coagulation, ozonation, and ferrous iron-catalyzed ozonation. Journal of Hazardous Materials. 2001;85(3):229-41. https://doi.org/10.1016/S0304-3894(01)00232-1
8. Lau W-J, Ismail AF. Polymeric nanofiltration membranes for textile dye wastewater treatment: Preparation, performance evaluation, transport modelling, and fouling control - a review. Desalination. 2009;245(1):321-48. https://doi.org/10.1016/j.desal.2007.12.058
9. Zhou Y, Lu J, Zhou Y, Liu Y. Recent advances for dyes removal using novel adsorbents: A review. Environmental Pollution. 2019;252:352-65. https://doi.org/10.1016/j.envpol.2019.05.072
10. Matloob AM, El-Hafiz DRA, Saad L, Mikhail S, Guirguis D. Metal organic framework-graphene nano-composites for high adsorption removal of DBT as hazard material in liquid fuel. Journal of Hazardous Materials. 2019;373:447-58. https://doi.org/10.1016/j.jhazmat.2019.03.098
11. Dehghani MH, Yetilmezsoy K, Salari M, Heidarinejad Z, Yousefi M, Sillanpää M. Adsorptive removal of cobalt(II) from aqueous solutions using multi-walled carbon nanotubes and γ-alumina as novel adsorbents: Modelling and optimization based on response surface methodology and artificial neural network. Journal of Molecular Liquids. 2020;299:112154. https://doi.org/10.1016/j.molliq.2019.112154
12. Bhandari H, Garg S, Gaba R. Advanced Nanocomposites for Removal of Heavy Metals from Wastewater. Macromolecular Symposia. 2021;397(1):2000337. https://doi.org/10.1002/masy.202000337
13. Tara N, Siddiqui SI, Rathi G, Inamuddin, Asiri AM. Nano-engineered adsorbent for removal of dyes from water: A review. Current Analytical Chemistry. 2019;15. https://doi.org/10.2174/1573411015666190117124344
14. Eswaran M, Dhanusuraman D. Chitosan Based Nanocomposite Biosensors: A Recent Review. Sensor Letters. 2018;16:81-91. https://doi.org/10.1166/sl.2018.3925
15. Valiey E, Dekamin MG, Alirezvani Z. Melamine-modified chitosan materials: An efficient and recyclable bifunctional organocatalyst for green synthesis of densely functionalized bioactive dihydropyrano[2,3-c]pyrazole and benzylpyrazolyl coumarin derivatives. International Journal of Biological Macromolecules. 2019;129:407-21. https://doi.org/10.1016/j.ijbiomac.2019.01.027
16. Yuan S, Zhang P, Yang Z, Lv L, Tang S, Liang B. Successive grafting of poly(hydroxyethyl methacrylate) brushes and melamine onto chitosan microspheres for effective Cu(II) uptake. International Journal of Biological Macromolecules. 2018;109:287-302. https://doi.org/10.1016/j.ijbiomac.2017.12.063
17. Sirajudheen P, Nikitha MR, Karthikeyan P, Meenakshi S. Perceptive removal of toxic azo dyes from water using magnetic Fe3O4 reinforced graphene oxide-carboxymethyl cellulose recyclable composite: Adsorption investigation of parametric studies and their mechanisms. Surfaces and Interfaces. 2020;21:100648. https://doi.org/10.1016/j.surfin.2020.100648
18. Liu J-L, Qian W-C, Guo J-Z, Shen Y, Li B. Selective removal of anionic and cationic dyes by magnetic Fe3O4-loaded amine-modified hydrochar. Bioresource Technology. 2021;320:124374. https://doi.org/10.1016/j.biortech.2020.124374
19. Wu Z-C, Wang Z-Z, Liu J, Yin J-H, Kuang S-P. A new porous magnetic chitosan modified by melamine for fast and efficient adsorption of Cu(II) ions. International Journal of Biological Macromolecules. 2015;81:838-46. https://doi.org/10.1016/j.ijbiomac.2015.09.020
20. Ahmed MA, Ali SM, El-Dek SI, Galal A. Magnetite-hematite nanoparticles prepared by green methods for heavy metal ions removal from water. Materials Science and Engineering: B. 2013;178(10):744-51. https://doi.org/10.1016/j.mseb.2013.03.011
21. Chowdhury SR, Yanful EK, Pratt AR. Chemical states in XPS and Raman analysis during removal of Cr(VI) from contaminated water by mixed maghemite-magnetite nanoparticles. Journal of Hazardous Materials. 2012;235-236:246-56. https://doi.org/10.1016/j.jhazmat.2012.07.054